JACS
JOURNAL OF THE AMERICAN CHEMICAL SOCIETY
Article
pubs.acs.org/JACS

Chemistry of Aqueous Silica Nanoparticle Surfaces and the Mechanism of Selective Peptide Adsorption

Siddharth V. Patwardhan,[†,‡] Fateme S. Emami,[§] Rajiv J. Berry,[∥] Sharon E. Jones,[∥] Rajesh. R. Naik,[∥] Olivier Deschaume,[†,⊥] Hendrik Heinz,*[,§] and Carole C. Perry*[,†]

[†]Interdisciplinary Biomedical Research Centre, School of Science and Technology, Nottingham Trent University, Clifton Lane, Nottingham NG11 8NS, U.K.

[‡]Department of Chemical and Process Engineering, University of Strathclyde, 75 Montrose Street, Glasgow G1 1XJ, U.K.

[§]Department of Polymer Engineering, University of Akron, Akron, Ohio 44325-0301, United States

[∥]Materials and Manufacturing Directorate, Air Force Research Laboratory, Wright-Patterson Air Force Base, Ohio 45433, United States

[⊥]Unité POLY, Université Catholique de Louvain, Boltzmann A+2, Croix du Sud, 1, B-1348, Louvain-la-Neuve, Belgium

Supporting Information

ABSTRACT: Control over selective recognition of biomolecules on inorganic nanoparticles is a major challenge for the synthesis of new catalysts, functional carriers for therapeutics, and assembly of renewable biobased materials. We found low sequence similarity among sequences of peptides strongly attracted to amorphous silica nanoparticles of various size (15−450 nm) using combinatorial phage display methods. Characterization of the surface by acid base titrations and zeta potential measurements revealed that the acidity of the silica particles increased with larger particle size, corresponding to between 5% and 20% ionization of silanol groups at pH 7. The wide range of surface ionization results in the attraction of increasingly basic peptides to increasingly acidic nanoparticles, along with major changes in the aqueous interfacial layer as seen in molecular dynamics simulation. We identified the mechanism of peptide adsorption using binding assays, zeta potential measurements, IR spectra, and molecular simulations of the purified peptides (without phage) in contact with uniformly sized silica particles. Positively charged peptides are strongly attracted to anionic silica surfaces by ion pairing of protonated N-termini, Lys side chains, and Arg side chains with negatively charged siloxide groups. Further, attraction of the peptides to the surface involves hydrogen bonds between polar groups in the peptide with silanol and siloxide groups on the silica surface, as well as ion−dipole, dipole−dipole, and van-der-Waals interactions. Electrostatic attraction between peptides and particle surfaces is supported by neutralization of zeta potentials, an inverse correlation between the required peptide concentration for measurable adsorption and the peptide p*I*, and proximity of cationic groups to the surface in the computation. The importance of hydrogen bonds and polar interactions is supported by adsorption of noncationic peptides containing Ser, His, and Asp residues, including the formation of multilayers. We also demonstrate tuning of interfacial interactions using mutant peptides with an excellent correlation between adsorption measurements, zeta potentials, computed adsorption energies, and the proposed binding mechanism. Follow-on questions about the relation between peptide adsorption on silica nanoparticles and mineralization of silica from peptide-stabilized precursors are raised.

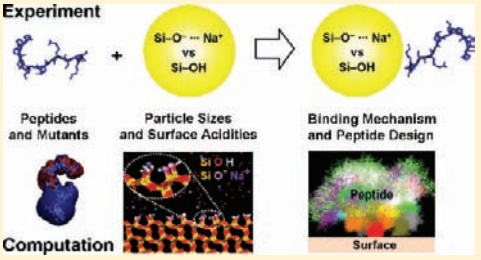

1. INTRODUCTION

Silica is an economically viable and technologically versatile material with applications in separation media, catalyst supports, biomedical materials, cosmetics, pharmaceuticals, detergents and coatings.[1] Biology has shown solutions to the controlled formation and assembly of hierarchical structures of silica and other biominerals *in vivo*, such as diatoms, mollusks, bones, and teeth, by use of peptides and proteins.[2,3] A common pathway toward tailored silica and other inorganic materials *in vitro*, therefore, has been the use of biological and synthetic organic molecules that are attracted to inorganic surfaces.[4] Biomolecules that facilitate the formation of silica include Lys, Arg, and Ser-rich peptides, poly lysine,[5,6] poly arginine,[7] R5 peptide from silaffin protein, and some recombinant proteins.[8,9] Thereby, the specificity and strength of inorganic−organic interactions affects the growth, shape, and stability of the assembled materials.[7,8,10] Insight into molecular interactions and control over resulting nanostructures remains, however, difficult to obtain.

A common approach to probe biomolecule−inorganic surface interactions is the use of combinatorial phage display libraries to identify strongly binding peptides for a given target material ("biopanning"). With this approach, peptides binding to a wide range of materials have been identified, including

Received: December 2, 2011
Published: March 21, 2012

 © 2012 American Chemical Society

metals and alloys, oxides, sulfides, selenides, zeolites, calcium carbonate, as well as organic compounds such as fullerenes, carbon nanotubes and polymers.[11] The specificity and strength of surface−peptide interactions has been attributed to the chemical nature of the surfaces; subtle differences in exposed crystallographic facets and in surface acidity; the structure, conformation, and flexibility of peptide backbones; as well as to interactions between the surfaces and water.[12−15] However, currently available instrumentation provides little direct insight into the surface environment and binding mechanisms. Even significantly different sequences of peptides with attraction to the "same" materials have been reported, for example, on silica[16−18] and metal surfaces.[13,19,20] The explanation of these data and control over selectivity requires characterization of the inorganic surfaces beyond past knowledge and insight into the binding mechanism (Figure 1).

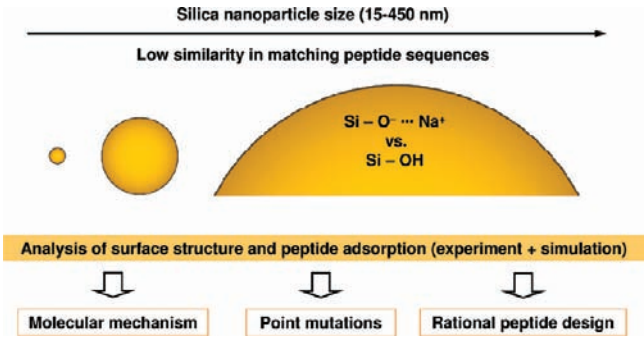

Figure 1. Motivation and aims of this work. We explain the attraction of highly dissimilar peptide sequences to different types of silica nanoparticles in phage display by differences in the surface structure. In particular, a significant increase in the surface acidity and in the area density of ionic groups with increasing size of silica nanoparticles derived from Stöber synthesis was found. The adsorption of purified peptides and mutants on uniformly sized silica particles was monitored using experimental techniques and atomistic simulation, suggesting an adsorption mechanism that involves ion pairing and hydrogen bonding. The results enable suggestions for the rational design of peptides for specific silica nanoparticles and remote relationships to silica mineralization.

The characterization of silica surfaces has involved X-ray Photoelectron Spectroscopy (XPS),[21,22] Fourier Transform Infrared Spectroscopy (FTIR, either DRIFTS or ATR),[21] Time-of-Flight Secondary Ion Mass Spectrometry (ToF-SIMS),[23] Extended X-ray Absorption Fine Structure (EXAFS), Sum Frequency Generation Spectroscopy (SFG), solid state NMR,[24] zeta potential measurements, and potentiometric titration.[25−34] XPS as a solid-state technique under vacuum is essentially limited to probe the chemical integrity of the silica nanoparticles. IR, ToF-SIMS, EXAFS, SFG, and NMR can further identify silicon environments on the nanoparticle surface (Q^4, Q^3, Q^2, Q^1, and Q^0) including the total density of silanol groups and sodium siloxide groups per surface area. The quantification of acid−base equilibria between silanol and siloxide groups on the surface in aqueous solution, however, requires potentiometric titration[25−34] or zeta potential measurements. Analysis of silica particles for chromatographic separations has shown that the surface density, acidity, and degree of ionization of silanol groups in solution depends on the synthetic origin and thermal history of the silica.[32] Different types of silanol groups on the surface of silica nanoparticles (single, vicinal, geminal) with distinct pK_a values determine the ionization state in aqueous solution as a function of ionic strength and pH. The density of sodium siloxide groups per surface area influences the concentration profile of the cations in the aqueous layer, the zeta potential, and the interaction with polar and charged peptides. The characterization of the aqueous silica interface and peptide binding, therefore, benefits from potentiometric titration, measurement of zeta potentials, peptide binding assays, IR spectroscopy, as well as molecular simulation with suitable force fields and surface models.[35−52] The wide range of possible surface structures of silica has been largely disregarded in previous studies on peptide binding[16−18] and in computer simulations.[35−37,40,42,43,45−47]

Molecular simulations have been previously helpful to identify the dynamics of peptides in solution, soft epitaxial adsorption on metal surfaces,[14,50,52] and self-assembly of surfactants on mineral surfaces in agreement with observations such as NMR, IR, XRD, DSC, AFM, TEM, and phage display.[38,41,44,48,51,53] The challenge of calculating protein structure on surfaces, however, is still that no published experimental structures are available to directly test and benchmark the accuracy of the predicted structures and the used force fields. The reliability of simulation results depends on factors such as the justification of surface models in comparison to experiment, the quality of the energy expression (force field), simplification of possible chemical reactions, and the sampling of the conformation space, particularly on the surface. For the simulation of inorganic−organic interfaces, approaches on the basis of thermodynamic consistency of the force field parameters for minerals, water, and biomolecules yield good results[41,44,54] while other approaches may involve high uncertainties.[35−37,40,42,43,45−47] While direct testing against experimental data can sometimes be a challenge, common force fields such as AMBER, CHARMM, and PCFF reproduce folding of short peptides up to 10 amino acids in aqueous solution acceptably, and compatible extensions for some minerals reproduce known surface tensions, interface tensions, and hydration energies.[41,44,54] We utilize a new force field for silica (PCFF-SILICA) that was tested to reproduce interface tensions of silica−aqueous interfaces as well as interfacial properties of related layered silicates, along with models of silica surfaces of appropriate surface acidity.

The organization of this paper is as follows. Following a summary of experimental and computational methods (section 2), we describe the synthesis of amorphous silica nanoparticles of three sizes (15, 82, and 450 nm)[55,56] and their differential affinity toward peptides in biopanning (section 3.1). Details of the surface structure and surface charge of the silica nanoparticles are then reported on the basis of surface titration, measurement of zeta potential, and molecular dynamics simulation (section 3.2). The binding mechanism of the phage-free, synthesized peptides is elucidated from binding assays on the same batch of 82 nm silica nanoparticles, measurements of zeta potentials, XPS analysis, IR spectroscopy, and simulation (sections 3.3 and 3.4). Further binding assays for mutant peptides are discussed to test the impact of changes in sequence, validate the adsorption mechanism, and guide in rational sequence design (section 3.5). We also report the activity of the same peptides in silica mineralization from molecular precursors, discuss follow-on questions on mineralization efficiency (section 3.6), and present conclusions in section 4.

2. MATERIALS AND METHODS

2.1. Experimental Methods. Reagents are described in section S1.1 of the Supporting Information. Silica particles of three sizes (15.0 ± 0.4, 82.0 ± 3.6, and 450 ± 22 nm) were prepared by a modified Stöber route and acid treated to yield hydroxy-terminated surfaces by removal of unreacted surface ethoxy groups.[55,56] Transmission electron microscopy (TEM) was used to measure particle size with a minimum of 40 particles for each sample measured. The same batch of particles was used

dx.doi.org/10.1021/ja211307u | J. Am. Chem. Soc. 2012, 134, 6244−6256

throughout this study. Peptide sequences binding to these silica samples were identified using combinatorial phage display libraries (12-mer and 7-mer) at pH 7.5 following previously described procedures of incubation, washing, cloning, and sequencing.[16] Lyophilized pure peptides for binding studies were either purchased from Sigma-Aldrich or synthesized in-house by microwave-assisted solid phase synthesis (CEM Discover SPS Microwave Peptide Synthesizer). Routine procedures for solid-phase peptide synthesis were employed,[57] using Wang resins preloaded with the Fmoc-protected C-terminal residue. Deprotection was carried out using piperazine in dimethylformamide; *O*-benzotriazole-*N*,*N*,*N*′,*N*′-tetramethyl-uronium-hexafluoro-phosphate and *N*,*N*-diisopropylethylamine were used as activator and activator base, respectively, for coupling amino acids; trifluoroacetic acid/thioanisole/3,6-dioxa-1,8-octanedithiol/water solution was used for cleaving peptides from the resin. The purity of lyophilized peptides was determined to be >90% by using a combination of High Performance Liquid Chromatography, ^{1}H-Nuclear Magnetic Resonance Spectroscopy, and Mass Spectrometry.

For the peptide-silica binding experiments, silica particles at a concentration of 1 mg mL^{-1} were suspended in phosphate buffered saline (50 mM phosphate, 150 mM NaCl, pH 7.5) by sonication for 1 h. pH and concentration of silica in the binding experiments were matched to those used in the biopanning experiments. The desired peptide was added to the silica solutions, mixed thoroughly by vigorous shaking and left standing for 1 h incubation before performing peptide quantification and ζ-potential measurements. To quantify the amount of adsorbed peptide, the amount of nonadsorbed, free peptide in solution after centrifugation was measured using a fluorescamine assay.[58] A comparison with other methods is discussed in section S1.2 of the Supporting Information. For this sensitive assay, a 180 μL aliquot of the supernatant obtained after centrifugation of the silica–peptide samples (13 000 rpm for 5 min) was dispensed into a 96-well cell culture plate. To this aliquot, 20 μL of fluorescamine in acetone (~15× in excess) was dispensed and mixed immediately prior to the measurement of fluorescence intensity using a Tecan Spectrafluor XFLUOR4 fluorescence intensity reader with a 360 nm excitation filter and a 465 nm absorption filter. Characterization of bound peptides by ATR-FTIR is described in section S1.3 of the Supporting Information. The measurement of the ζ-potential of silica particles with and without the presence of peptides was performed using a Zetasizer Nano ZS from Malvern Instruments using a disposable capillary cell. Typically, 1 mL aliquots of each sample were injected into the capillary cell and 5–10 measurements per sample were performed at 25 °C.

The activity of peptides in silica synthesis was studied using either dipotassium silicon catecholate (SiCat) or tetramethyl orthosilicate (TMOS) precursors by monitoring the condensation kinetics as well as the collection of precipitates. The condensation was quantified using the well-established molybdosilicate assay as described elsewhere.[9] Details on mineralization, characterization of silica–peptide hybrids, and error analysis are given in sections S1.4 and S1.5 in the Supporting Information.

2.2. Computational Methods. Classical molecular dynamics simulation in all-atomic resolution was employed for the analysis of silica–water interfaces and the binding mechanism of peptides on the molecular scale,[59,60] including density profiles, visualization of adsorbed peptides over time, adsorption energies,[48] Ramachandran plots, and computed NMR spectral shifts.[61] Details of the models, force field parameters and new developments for silica (polymer consistent force field augmented for silica, PCFF-SILICA), simulation setup, and analysis are described in section S2 of the Supporting Information.

The simulation relies on a classical Hamiltonian with thermodynamic consistency between the inorganic and organic components. Computed surface and interface energies of silica were tested to be in agreement with experiment,[38,39,41,44,50,53] which is an improvement over earlier models that are associated with deviations up to 500% in interfacial energies and high uncertainties in interfacial structure and dynamics.[35−37,40,42,43,45−47] We utilized models of even Q^3 and Q^2 silica surfaces of approximately 3 × 3 nm^2 to 5 × 5 nm^2 size with a surface density of silanol plus siloxide groups corresponding to 4.7 and 9.4 groups/nm^2, respectively, in agreement with experimental findings.[32,33] The fraction of silanol groups ionized to sodium siloxide groups varied as 0%, 9%, 18%, 25%, and 50% in correspondence to experimentally observed degrees of ionization depending on pH and particle size.[25−31] We employed between 1600 and 5000 water molecules and peptides in the zwitterionic state corresponding to pH ~ 7.5. For each combination of silica surface and peptide, at least 10 independent molecular dynamics simulations of ≥5 ns duration were carried out in the NPT and NVT ensembles using the Materials Studio graphical interface[60] and the program LAMMPS.[59] A high level of convergence in equilibrium structures and energies was reached for analysis (see section S2 in the Supporting Information).

3. RESULTS AND DISCUSSION

3.1. Uniqueness of Peptides Identified by Biopanning. Sequences of many silica-binding peptides were reported in three previous biopanning studies;[16−18] however, the similarity score among the peptides is low. The studies employed silica–peptide hybrid particles and gels prepared in aqueous solution,[16] thermally grown silicon oxide,[17] and crystalline quartz particles,[18] all of which differ in bulk structure, bulk chemistry, surface structure, and surface chemistry. A common substrate characterization as "silica", therefore, appears too simplistic, resulting in low sequence similarity of the peptides and lack of a consensus sequence.

To understand differences in surface structure and in peptide binding, we synthesized amorphous spherical silica particles of three sizes (15, 82, and 450 nm diameter) using a modified Stöber procedure[55,56] and subjected the particles to biopanning. Tightly bound phages were eluted, cloned, and sequenced (Table 1).

Table 1. Sequences and Properties of Peptides Identified as Tight Binders to Silica Particles

Particle size (nm)	Peptide name	Peptide sequence	Occurrence[a]	pI[b]
15.0 ±0.4	pep2	YITPYAHLRGGN	14/20	8.6
82.1 ±3.6	pep1	KSLSRHDHIHHH	20/20	8.8
	7mer	LDHSLHS	16/20	6.0
450 ±22	pep4	MHRSDLMSAAVR	20/20	9.4
Bioinspired silica ~500[c]	Si4-1	MSPHPHPRHHHT[d]	NA	9.6
	Si4-10	RGRRRRLSCRLL[d]	NA	12.3

[a]Number of the sequences of clones out of 20 sequenced peptides after fifth round of washing. [b]Estimated using Expasy's ProtParam tool with an accuracy of ±0.1 units (ref 66). [c]This silica sample was prepared using R5 peptide derived from the silaffin proteins of diatoms (ref 16). [d]These peptide sequences were reported earlier and are included here for comparison (ref 16).

While all target materials are "amorphous silica particles" with negligible curvature at the peptide length scale (2–3 nm), the sequences of the identified peptides display less than 25% similarity in amino acid composition (Table S2).[62] Peptide pep1 with strong attraction to silica particles of 82 nm diameter is also less than 42% similar to peptide Si4-1 which was previously reported as a silica binder.[16] These findings strongly support the sensitivity of peptide–silica interactions to surface environments that depend on the synthetic origin of silica nanoparticles.[32,63] The apparent existence of many 'tight silica binders' is a major difference to surfaces of silver, gold, and GaAs for which consensus sequences were reported after five rounds of biopanning.[64] Such surfaces may still display different crystal facets (*hkl*) that attract distinct peptides;[14,20,50,65] however, they are not exposed to hydration–dehydration reactions and to pH sensitive acid–base equilibria as silica.

3.2. Surface Properties of Silica Nanoparticles. The surface chemistry of the amorphous silica particles is, therefore, dependent on the surface topography; the distribution of Q^4, Q^3, and Q^2 environments; and the distribution of siloxane

dx.doi.org/10.1021/ja211307u | J. Am. Chem. Soc. 2012, 134, 6244−6256

(Si−O−Si), silanol (Si−OH), and ionic siloxide (Si−O$^-$···Na$^+$) groups.[25−34] Attenuated Total Reflection Fourier Transform Infrared Spectroscopy (ATR-FTIR) on the surface of the differently sized silica particles indicates very similar band positions and relative intensities (Figure S2), corresponding to the same ratio of Si−O−Si groups to (Si−OH and Si−O$^-$ Na$^+$) groups. Earlier studies have shown that XPS and EXAFS measurements yield limited additional information about the surface structure.[21,22] A recent paper[22b] concludes that "noticeable differences in (hydrated and dehydrated) spectra brings into question the significance of ex situ molecular probes to accurately describe the solid-liquid interface". The surface acidity and fraction of anionic siloxide groups per surface area follow from earlier potentiometric titrations[25−32] and measurements of the zeta potential as a function of pH (Figure S3). A thermally unprocessed Q^3 silica surface usually contains 4.7 silanol groups/nm^2 of which 4% to 21% are deprotonated at pH ∼ 7.5 depending on the synthetic origin and on the total ionic strength in solution.[25−32]

Potentiometric data rely on the uptake of added electrolytes on the surface of the silica nanoparticles such as HCl at low pH or NaOH at high pH. A comparison of the required amount of electrolyte to change the pH of the colloidal solution with particles versus the required amount of electrolyte to change the pH of the dialysate containing no particles indicates a negative charge between 0.21 and 1.0 siloxide groups/nm^2 surface area at pH ∼ 7.5.[25−31] For silica sol at pH ∼ 7.5 and an ionic strength of 0.1 M, the reported numbers of siloxide groups per nm^2 are 0.33 by Bolt,[24] 0.21 by Milonjic,[28] and 0.56 by Zerrouk and co-workers.[29] Surface charge measurements of BDH precipitated silica samples at pH ∼7.5 and ionic strength of 0.1 M indicated a siloxide density of ∼0.75 per nm^2 by Yates et al.[27] and between 0.56 and 1.0 per nm^2 by Tadros and co-workers.[25] The wide distribution of the degree of ionization indicates the sensitivity of the surface chemistry of silica to synthesis and preparation conditions, especially under consideration of the small experimental uncertainty of ±0.01 siloxide groups/nm^2 in the above studies.[25−31]

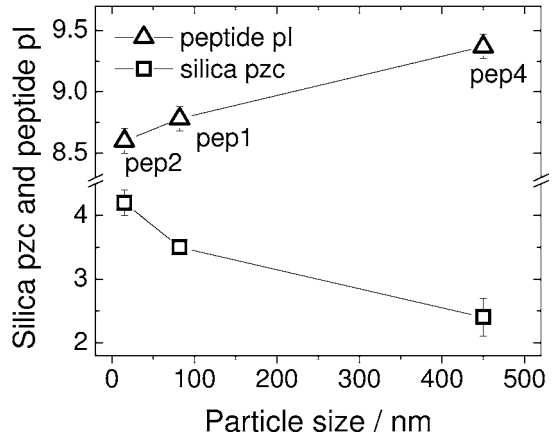

Figure 2. Point of zero charge of silica samples and p*I* of peptides attracted as a function of particle size. The more acidic the silica surface, the more alkaline peptides are preferentially adsorbed.

In the modified Stöber synthesis of silica nanoparticles in this study, the concentration of ammonia was varied to control particle size.[55,56] Higher ammonia concentration precipitates larger particles, ionizes more silanol groups, and leads to higher surface

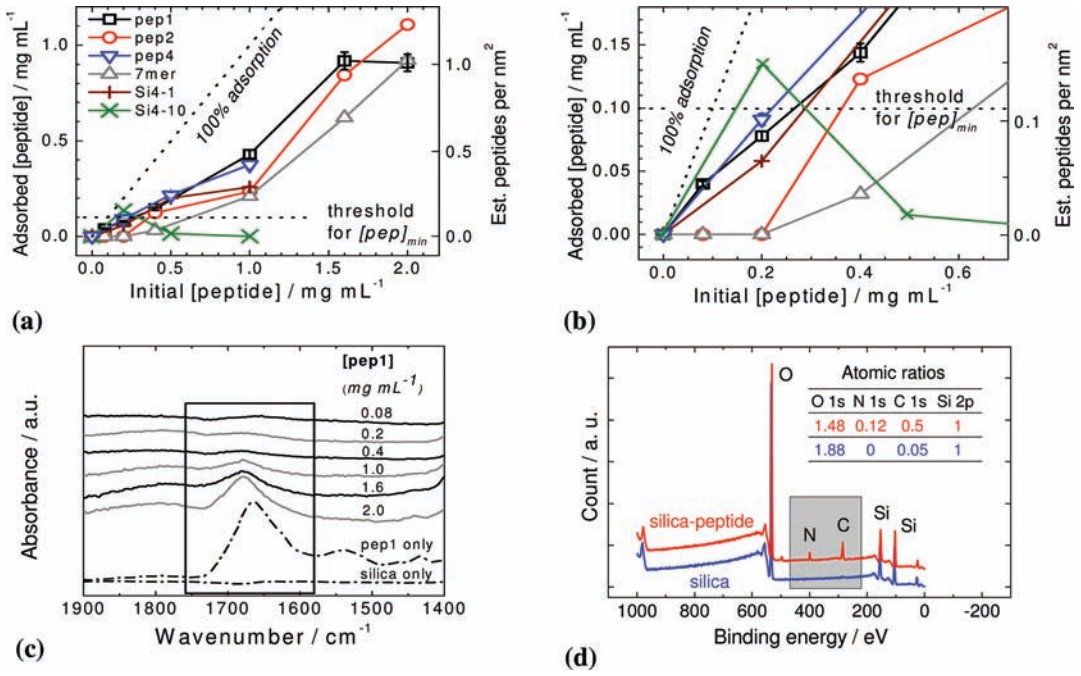

Figure 3. (a) Adsorbed amount of peptides on 82 nm silica particles as a function of initial peptide concentration. The inclined dotted line indicates hypothetical adsorption of all peptide added to the solution. The horizontal dotted line aids in the determination of an initial peptide concentration threshold $[pep]_{min}$ for significant adsorption well below monolayer coverage. The error bars are small and indicate a 95% confidence interval. (b) Magnification of graph in (a) for low peptide concentrations. (c) ATR-FTIR spectra of the silica samples containing adsorbed peptide Pep1 for a range of initial peptide concentrations. ATR-FTIR is less sensitive compared to the fluorometric assay in panels a and b so that characteristic amide bands of adsorbed peptides between 1600 and 1750 cm^{-1} can only be seen at initial peptide concentrations in excess of 1 mg/L (see highlighted box).

dx.doi.org/10.1021/ja211307u | *J. Am. Chem. Soc.* 2012, 134, 6244−6256

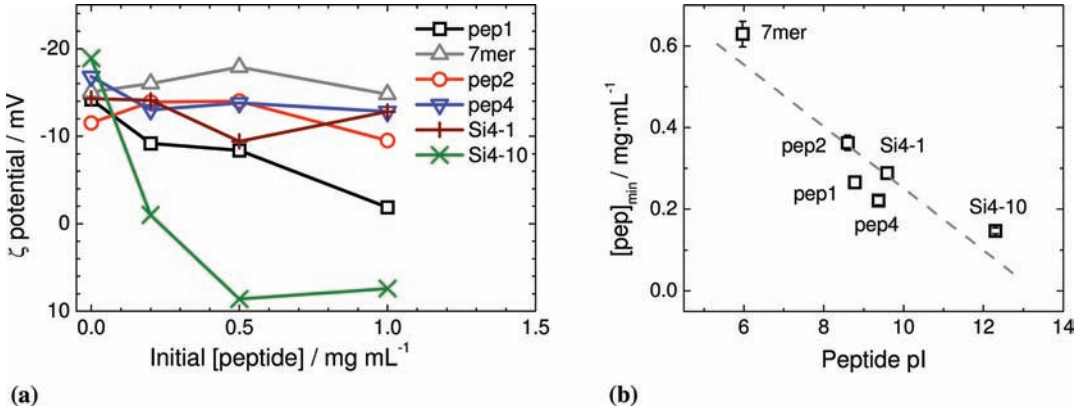

Figure 4. (a) The ζ-potential of silica particles in the presence of peptides as a function of initial peptide concentration. (b) Correlation between peptide pI and the initial peptide concentration threshold $[pep]_{min}$ to induce significant adsorption below monolayer coverage. The dashed line shows a linear fit with $R^2 = -0.918$.

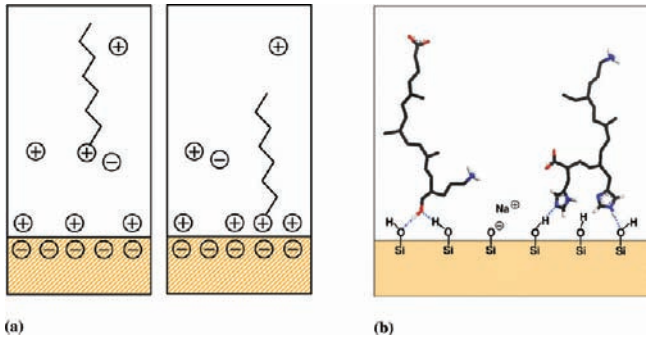

Figure 5. Major contributions to the adsorption of peptides on silica surfaces. (a) Formation of ion pairs, in which cationic peptide residues coordinate unoccupied anionic surface sites. (b) Hydrogen bonds and other polar interactions between groups in the peptide and silanol/siloxide groups on the surface.

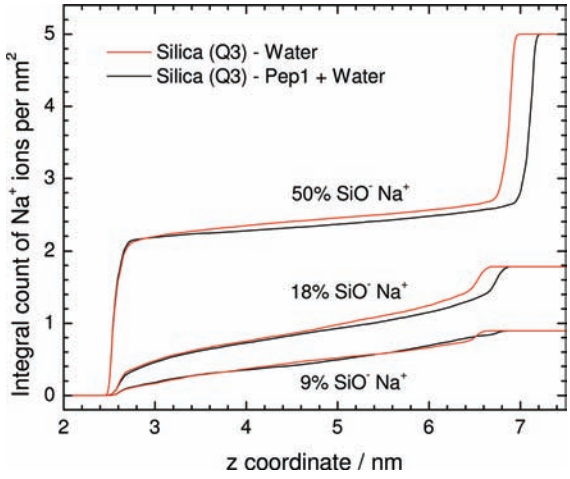

Figure 6. Average position of sodium ions on silica–water and silica–peptide–water interfaces for different degree of ionization of even Q^3 silica surfaces in molecular simulation (average over 20 ns). The total density of ionizable silanol groups is ~5 per nm^2, and the integral over the area density of Na^+ ions is shown as a function of distance from the surface at $z \sim 2.5$ nm (a second surface at $z \sim 6.8$ nm is also present). The degree of dissociation of sodium ions into the solution phase is minimal at high degree of ionization and increases toward lower degree of ionization. The adsorption of cationic peptides such as pep1 does not change the distribution of Na^+ ions in solution, in support of the formation of ion pairs between cationic residues and surface siloxide groups rather than ion exchange. The thickness between the two surfaces increases slightly in the presence of peptide due to the added molecular volume.

acidity. The effective pK_a value of the superficial silanol groups is thus lower for larger nanoparticles, possibly supported by a higher fraction of vicinal silanol groups and better stabilization of siloxide anions by hydrogen bonds. Lower concentration of ammonia precipitates smaller particles, ionizes less silanol groups, and the surface acidity is lower. Titration of the silica particles with NaOH from pH ~2 to ~12 under simultaneous measurement of the ζ-potential (Figure S3) shows a positive ζ-potential for pH < 2–4, corresponding to a surface consisting of silanol groups and protonated silanol groups.[67] The ζ-potential reaches zero around pH ~ 2–4 when the surface is covered entirely by silanol groups. A negative ζ-potential is found for further increase in pH due to the formation of sodium siloxide groups until the particles begin to dissolve at pH >8. The point of zero charge (pzc) decreased from 4.2 to 2.4 as the size of the silica particles increased from 15 to 450 nm, in agreement with the increased acidity and ionization of larger silica particles (Figure 2). The increased surface density of negatively charged siloxide groups on larger nanoparticles also attracted phage-bound peptides with a higher pI value, that is, with a higher number of positively charged residues such as ammonium or guanidinium groups in lysine (K) or arginine (R) (Figure 2). This trend indicates electrostatic contributions to binding[68] and recognition of the surface chemistry of the peptides.[69]

3.3. Measurement of Peptide Binding and Binding Mechanism. Binding assays were then performed for the six synthetic peptides in Table 1 on a single batch of silica particles of diameter of 82 nm. The choice of one particle size and peptides without virus eliminates any uncontrolled factors in previous studies.

We include the previously identified peptides Si4-1 and Si4-10 due to their ability for binding to silica as well as for silica mineralization from hydrolyzed solutions of alkoxysilanes.[16] The virus-attached peptides were the strongest binders to networks of spherical composite nanoparticles of ~500 nm size (derived from silica precursors and R5 peptide) among several sequences identified by biopanning, whereby Si4-1 precipitated high amounts of networks of silica particles of 250–500 nm size while Si4-10 exhibited very little or no silica precipitation.[16]

Fluorometric analysis was employed to quantify the amount of peptide adsorbed to the silica particles as a function of concentration (Figure 3a,b). In addition, ATR-FTIR confirmed the adsorption of

dx.doi.org/10.1021/ja211307u | J. Am. Chem. Soc. 2012, 134, 6244–6256

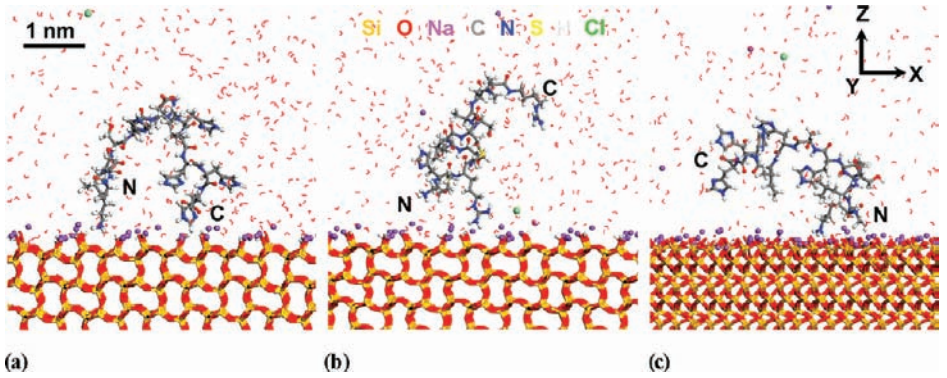

Figure 7. Snapshots of the peptides adsorbed on silica surfaces in aqueous solution in all-atomic detail. The location of N- and C-termini is highlighted. (a) Pep1 on a Q^3 silica surface, (b) pep4 on a Q^3 silica surface, (c) pep1 on a Q^2 silica surface (50% ionization). The peptides are mainly bound to the surface by Lys, Arg, Ser, and sometimes His residues. Lys residues attach more strongly to the charged surfaces than Arg. Ser and His approach the surface intermittently. Note the occurrence of larger and smaller grooves on the regular Q^3 silica surface in panels a and b.

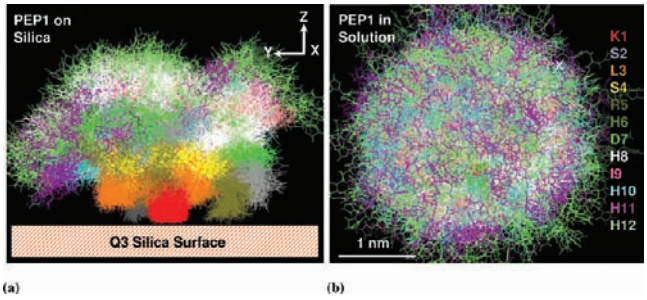

Figure 8. Superimposed conformations of peptide pep1 (a) on a Q^3 silica surface and (b) in solution. The images are color-coded by amino acid residue. The image on the surface shows approximately 1000 peptide conformations over a simulation time of 20 ns in which peptides were closest to the surface. The center of mass of K1 residues was laterally translated for ease of structural comparison. The image of pep1 in solution was generated from 2000 conformations by alignment of residue K1 using 3D translation and rotation. The superposition illustrates an isotropic structure in solution which is similarly found for the other peptides.

peptides at initial concentrations above 1 mg/L (Figure 3c). XPS analysis of dried samples demonstrated the clean composition of neat silica nanoparticle surfaces as well as the presence of peptide upon adsorption, showing signals of nitrogen and carbon (Figure 3d, Figure S4a,b). The adsorption isotherms in aqueous solution differ significantly from peptide to peptide (Figure 3a,b). Common is an initial increase in adsorption with increasing peptide concentration. The onset of adsorption was immediate for pep1, pep4, Si4-1, and Si4-10, while higher concentrations were required for pep2 and 7mer. The increase in adsorption at higher initial concentrations appears to level off somewhat for the first group of peptides (pep1, pep4, Si4-1, Si4-10), and specifically reverses for Si4-10 which is strongly cationic due to six R residues (see Table 1). On the other hand, the increase in adsorption at higher initial concentrations intensifies for pep2 and 7mer. We can discern different behavior of cationic and noncationic peptides, as the peptides in the first group are cationic (higher p*I*) and the peptides in the second group are closer to neutral or anionic (lower p*I*).

The attraction of cationic peptides pep1, pep4, Si4-1, and Si4-10 at low initial concentration <0.2 mg/L can be related to ion pairing with negatively charged siloxide groups on the silica surface. This view is supported by the reduction of the negative ζ-potential of the negatively charged silica surface with increasing initial peptide concentration (Figure 4a) and a steady increase in the adsorbed amount (Figure 3a,b). Peptide Si4-10 with multiple

Table 2. Sequence of Wild-Type Peptide Pep1 and the Two Variants Pep1_6 and Pep1_11 in Which H6 or H11 Was Replaced by Alanine[a]

Peptide	Sequence	pI
pep1	KSLSRHDHIHHH	8.8
Pep1_6	KSLSRADHIHHH	8.8
pep1_11	KSLSRHDHIHAH	8.8

[a]The p*I* was estimated using Expasy's ProtParam tool.

positive charges even reverses the silica surface charge to positive values above 0.2 mg/L initial concentration, related to partial coverage of the surface with peptide and its multiple positively charged arginine side chains. The hypothesis of ion pairing is also consistent with a low initial peptide concentration threshold $[pep]_{min}$ that leads to significant adsorption below monolayer coverage (Figure 4b). Peptide monolayer coverage could be reached at or above approximately 0.3 mg/L adsorbed peptide or ~0.3 adsorbed peptides/nm^2,[70] and we define the minimum initial concentration threshold of a peptide $[pep]_{min}$ that leads to an adsorbed amount greater than 0.1 mg/mL as an indicator for significant peptide adsorption (Figure 3a,b and Figure S4c). We then find lower concentration thresholds $[pep]_{min}$ for increasing peptide p*I* (Figure 4b), in support of stronger attraction of cationic peptides to the anionic silica surface by ion pairing or ion exchange. The observations for cationic peptides thus illustrate electrostatic contributions to adsorption (Figure 5a).

Peptides with lower p*I* such as pep2 and the anionic peptide 7mer also bind to the silica surface. At low initial concentration <0.2 mg/L, weak or no adsorption occurs as there are hardly cationic groups available to form ion pairs with siloxide groups on the particle surface. However, the peptides do adsorb after a certain initial peptide concentration threshold is reached (Figure 3a,b). Upon adsorption, we notice only small or no reduction in ζ-potential which suggests adsorption through hydrogen bonds and polar interactions, rather than by ion pairing or ion exchange (Figure 4a). Since hydrogen bonds are weaker than electrostatic interactions, adsorption requires a higher initial peptide concentration threshold $[pep]_{min}$ for significant adsorption (Figure 4b). Therefore, we can distinguish hydrogen bonds and polar interactions as a second important contribution to adsorption (Figure 5b).

When the initial concentration of the peptides increased to higher values above ~1 mg/L, adsorption of cationic peptides could level off due to surface neutralization and an increase in peptide−peptide electrostatic repulsion (Figure 3a). Then, the

dx.doi.org/10.1021/ja211307u | J. Am. Chem. Soc. 2012, 134, 6244−6256

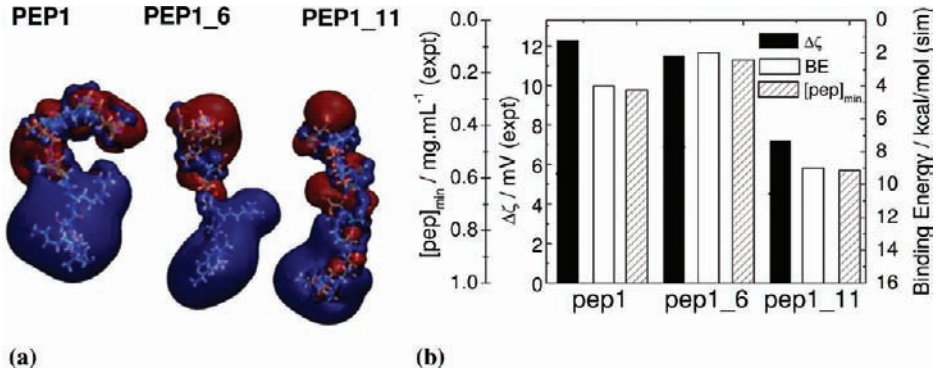

Figure 9. Properties of pep1 and its variants pep1_6 and pep1_11. (a) Secondary structure and distribution of cationic (blue) and anionic (red) potentials on the peptide backbone in aqueous solution. (b) Comparison of the initial peptide concentration threshold $[pep]_{min}$ for significant binding (LHS), the change in zeta potential $\Delta\zeta$ upon increase of the initial peptide concentration from 0 to 1 mg/mL (LHS) and the computed binding energies in dilute aqueous solution (RHS).

surface might be saturated with a first (or second) peptide layer. The adsorption of less cationic peptides such as pep2 and 7mer, in contrast, could increase even further at elevated initial concentration without saturation, in support of the formation of hydrogen bonded multilayers (Figure 3a). It may then be favorable for the peptide to bind to a peptide-covered surface. In addition, also cationic peptides experience hydrogen bond and polar interactions with the surface, so that surface attraction likely involves ion pairing and hydrogen bonds simultaneously (Figure 5). As an extreme, however, peptide Si4-10 with many positive charges binds strongest at very low concentration due to ion-pairing whereas peptides pep1, pep4, and Si4-1 with only one positive net charge bind weaker (Figure 3b). Also, Si4-10 shows a clear trend toward surface saturation and even avoids monolayer formation due to repulsion of the spatially dense cationic groups (Figures 3a, 4a). Detachment from the surface at higher concentrations still leaves open questions. Several explanations appear possible,[71] including the formation of peptide clusters in solution that contribute to a positive zeta potential.

The data are well supported by the proposed adsorption mechanism while some uncertainties remain. Strong support comes from similar mechanistic trends for the adsorption of ionic and noncharged surfactants to oppositely charged and neutral surfaces,[68] as well as for the adsorption of dissolved solutes onto heterogeneous nanostructured materials.[72] The specificity of peptide–surface interactions clearly leads to adsorption isotherms very different from Langmuir isotherms with exponential saturation.[69] Alternative adsorption mechanisms may involve multistep processes[73] and joint deposition of peptide aggregates after the peptides have preformed aggregates in solution at sufficiently high initial concentration.

3.4. Characterization of Silica–Water Interfaces and Peptide Binding by Molecular Simulation. Atomistic simulation of the silica surfaces in contact with water and peptides provides insight at the nanometer scale into the possible structure of the interfaces and the binding mechanism (Figures 6–8). As a first approximation, we employed even Q^3 and Q^2 silica surfaces of 3×3 to 5×5 nm^2 size which are 3–10 times larger than the maximum surface area covered by the single peptides.

To understand the influence of increasing surface ionization of the silica nanoparticles with increasing particle diameter (Figure 2), we assumed models of Q^3 silica surfaces in contact with water with different degrees of ionization of the silanol groups (Figure 6, Figures S5, S6). The different aqueous interfaces exhibit significant structural differences in molecular dynamics simulation. A high area density of sodium siloxide groups (50%) leads to close proximity of most sodium cations to the surface and only a small fraction of the cations dissociates into solution. Surfaces with a lower density of sodium siloxide groups (18% and 9%) release a higher fraction of sodium ions into solution, up to near quantitative dissociation. The penetration of cations into solution then exceeds several nanometers, and the superficial layer of water and cations reminds of swollen clay minerals.[74] As the area density of sodium siloxide groups approaches zero (no cations), the surface becomes electrically neutral. This trend reveals a maximum number of freely dissociated, mobile cations per surface area for intermediate degrees of ionization near 20% or one siloxide group per nm^2.

These differences in cation dissociation (Figure 6) explain the measured zeta potentials of the silica nanoparticles at pH 7.5 in a qualitative way (Figure S3). Highly ionic surfaces exhibit a low degree of cation dissociation and therefore do not display the largest zeta potential upon application of an electric field (−35 mV for most acidic silica nanoparticles of 450 nm size). Intermediately ionic surfaces show the largest number of dissociated, mobile cations per surface area and thus the largest zeta potential (−40 mV for intermediately acidic silica nanoparticles of 82 nm size). Weakly ionized surfaces have a high degree of dissociation but fewer cations so that the zeta potential diminishes (−20 mV for weakly acidic silica nanoparticles of 15 nm size). Moreover, when the pH value approaches the point of zero charge, no cations are present in both simulation and experiment and the zeta potential is zero.

The results indicate that molecular dynamics simulation, zeta potential measurements (Figure 4a, Figure S3), and potentiometric titrations of silica surfaces (section 3.2)[25−34] converge to a consistent understanding of the chemistry of aqueous silica surfaces. In first approximation, Q^3 silica surfaces with ~4.7 silanol plus siloxide groups/nm^2 and between 0.2 and 1.0 ionic SiO^-Na^+ groups/nm^2 appear to be suitable models at pH ~ 7.5. The variation in the number of SiO^-Na^+ groups per nm^2 up to multiples depending on synthesis conditions of the silica nanoparticles leads to distinct surface environments and appears to be the main reason for the specific adsorption of dissimilar peptides (as reported in sections 3.1 and 3.2).

The mechanism of peptide adsorption to the silica surfaces can be monitored by changes in the interfacial structure and visual analysis. The density profile of sodium ions (Figure S6) and the integral of the sodium density remain essentially unchanged in the presence of pep1 and pep4 compared to the pure aqueous interface (Figure 6). Therefore, cationic groups in the peptide

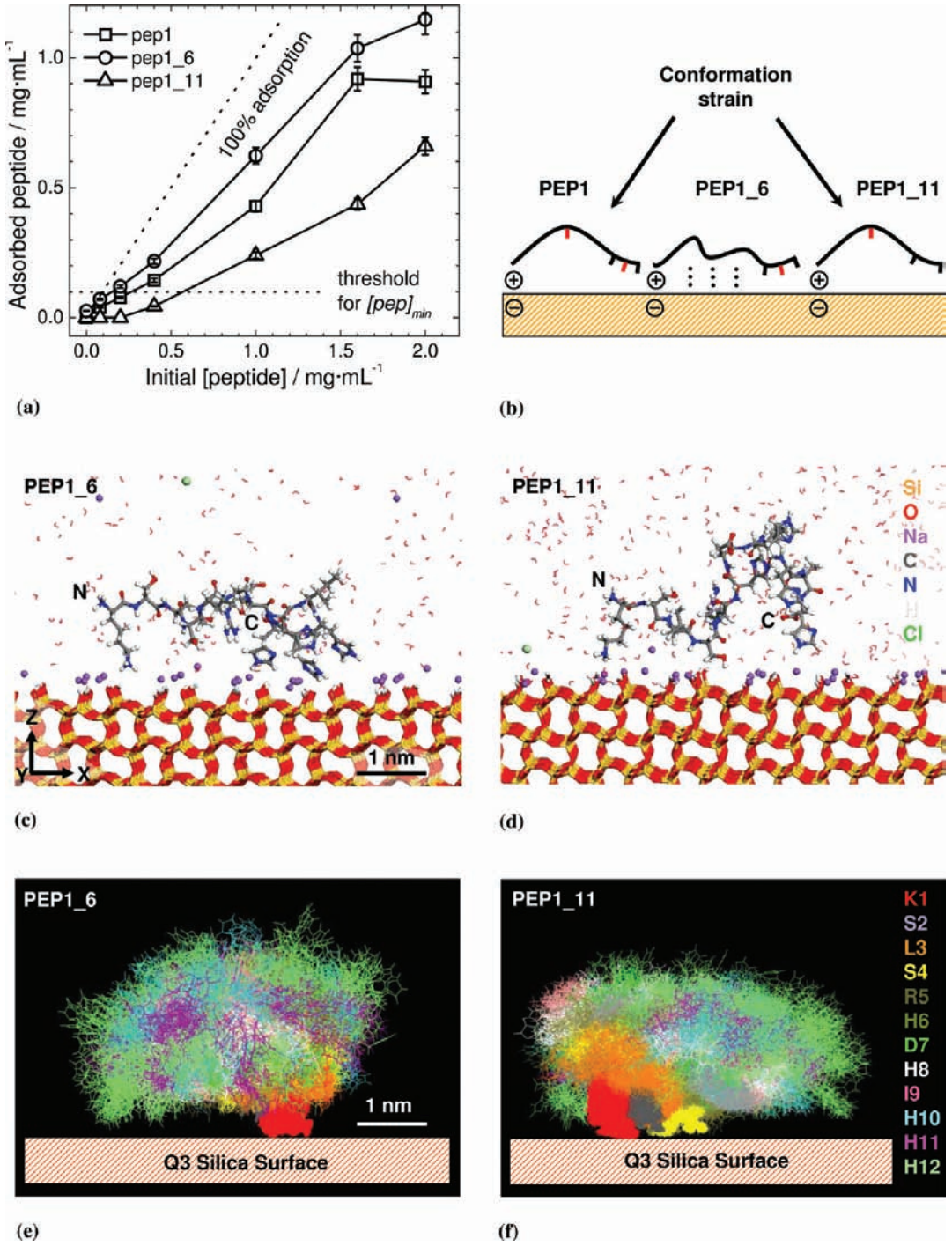

Figure 10. (a) Adsorption of pep1 and pep1 mutant peptides on 82 nm silica particles as a function of initial peptide concentration. (b) Schematic of the adsorbed peptides on the silica surface, illustrating the role of His-6 and His-11 (dashes along the backbone indicate His). The backbone of Pep1 is somewhat bent, partial protonation and hydrogen bonding attach the terminal His residues. Mutation of His-6 (blue) to Ala in pep1_6 reduces backbone stiffness, facilitates better ion pairing and more hydrogen bonds along the entire backbone, leading to stronger binding. Mutation of His-11 to Ala retains conformation strain in the middle section and decreases the number of hydrogen bonds due to loss of His-11, leading to weaker binding. (c and d) Snapshots of peptides pep1_6 and pep1_11 on Q^3 silica surfaces in aqueous solution in all-atomic detail (50% ionization). (e and f) Superposition of bound conformations of peptides pep1_6 and pep1_11 on the Q^3 silica surface. The images are color-coded by amino acid residue and show approximately 1000 peptide conformations in which peptides were closest to the surface over a simulation time of 20 ns. The center of mass of K1 residues was translated horizontally for ease of structural comparison.

coordinate with negatively charged surface sites by formation of ion pairs, and do not exchange surface-bound sodium ions (Figure 5a). This trend is also supported by visual analysis (Figures 7 and 8). The cationic peptide pep1 was found within a distance of <3 Å from the superficial SiOH/SiO^- layer of the surface during 70–80% of simulation time. Pep4 remained separated from the same surface by several water layers for 80% of simulation time. In bound conformations, N-terminal ammonium groups and ammonium groups on Lys side chains often approach major grooves near siloxide groups on the surface (Figure 7).[71] Guanidinium groups in

dx.doi.org/10.1021/ja211307u | J. Am. Chem. Soc. 2012, 134, 6244–6256

Table 3. Computed Adsorption Energies E_{ads} of Peptides on Regular Q^3 and Q^2 Silica Surfaces in Dilute Aqueous Solution[a]

peptide	pep1	Pep1_6	pep1_11	pep4
E_{ads} (kcal/mol) − Q^3	+4 ± 3	+2 ± 3	+9 ± 3	+7 ± 3
E_{ads} (kcal/mol) − Q^2	+14 ± 3	+12 ± 3	+1 ± 3	+1 ± 3

[a]Lower values correspond to stronger adsorption (see section S2 in the Supporting Infomation).

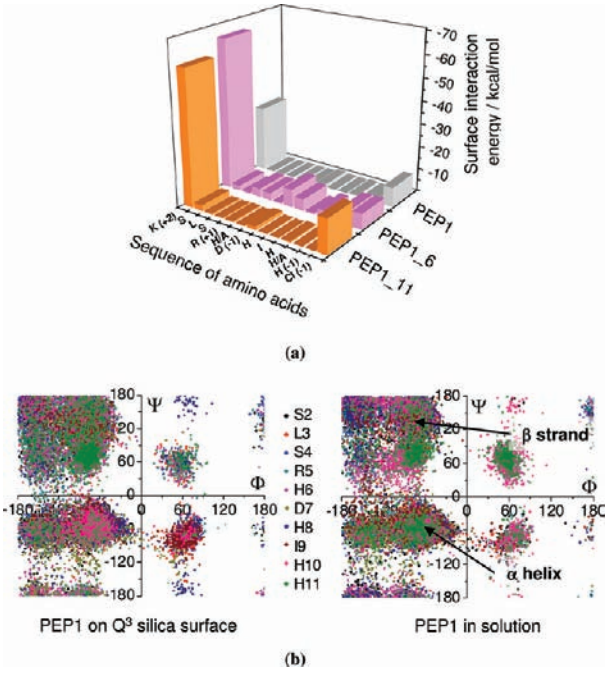

Figure 11. (a) Interaction energies of individual amino acids in pep1, pep1_6, and pep1_11 with the surface, disregarding contributions by water molecules. The interaction energies correlate with residue polarity and proximity to the surface. Replacement of H6 by A6 in pep1_6 facilitates significant interactions of several amino acids with the surface, resulting in strongest binding (Table 3). (b) A Ramachandran plot of pep1 on the Q^3 silica surface and in solution shows modest conformational changes. Each graph is based on 2000 data points per amino acid over a cumulative simulation time of 20 ns.

Arg side chains show the same trend in weaker form. The formation of ion pairs explains the reduction of silica surface charge and zeta potential upon binding of cationic peptides, and no such reduction occurs upon binding of neutral or negatively charged peptides such as pep2 and 7mer (Figure 4, Figure S7).

In addition to the formation of ion pairs, His, Ser, and Asp residues show intermittent contacts with the surface through hydrogen bonds. These contributions to adsorption were examined further on Q^3 silica surfaces covered by silanol groups only. The peptides then remained bound to the surface by hydrogen bonds and polar interactions, although with higher lateral mobility and an increased time-averaged distance from the surface of approximately 10 Å. Near the point of zero charge or in the absence of cationic groups, peptides may therefore still adsorb to the silica surface but require a higher minimum concentration $[pep]_{min}$ for significant binding to occur, as shown for pep2 and 7mer (Figure 3a,b).

In conclusion, the major contributions to binding are ion pairing and hydrogen bonds, as well as less energetic ion−dipole, dipole−dipole, and van-der-Waals interactions (Figure 5). The balance of the two major contributions depends on the p*I* and conformational flexibility of the peptides. The peptides on the surface also exhibit a rich dynamics over time which we chose to represent as a time average by superposition of equilibrium structures (Figure 8). We also note that further investigations will be required to study the impact of the surface topology of amorphous silica nanoparticles (flat, rough, porous), the detailed balance of bonding environments (Q^4, Q^3, and Q^2), the ratio between silanol and siloxide groups (according to synthetic origin, pH, ionic strength), as well as of the kind of silanol/siloxide groups (isolated, vicinal, geminal, dependence on topology). The advantage of computer models in comparison to experiment is that these aspects of surface structure can be controlled and systematically varied.

3.5. Influence of Point Mutations on Binding. We selected a limited set of two mutants derived from pep1 to explain the importance of particular residues for interfacial interactions and peptide−silica binding (Table 2). We focused on histidine motifs which are believed to play a critical role in binding,[17] frequently found in *in vivo* and in *in vitro* silica binding peptides,[16,17,75] and known for their ability to form hydrogen bonds between the imidazole groups and superficial silanol and siloxide groups on silica surfaces. The two chosen mutants are pep1_6 by replacement of His-6 to Ala-6 in pep1 and pep1_11 by replacement of His-11 to Ala-11 in pep1 (Table 2). This choice was supported by (i) ease of folding and lower molecular energy of pep1_6 during MD simulation in aqueous solution compared to pep1 and pep1_11 (Figure S8), (ii) mutation of His-11 rather than His-10 or His-12 to preserve a distance from the negatively charged C-terminal (H-12) that could be electrostatically repelled from the surface, and to retain more rotational freedom compared to replacement of His-10. Pep1 and pep1_6 showed similar distributions of electrostatic potential comprising two well-defined domains while pep1_11 showed an alternating distribution of electrostatic domains (Figure 9a). The mutants pep1_6 and pep1_11 were synthesized and exposed to 82 nm silica particles to assess their adsorption using fluorometric binding assay, changes in zeta potential, and by MD simulation (Figures 9b and 10).

The adsorption isotherms of the three peptides pep1, pep1_6 and pep1_11 exhibit significant differences (Figure 10a). For the same p*I* values, substitution of His-6 in the middle for Ala (pep1_6) increased adsorption on silica and reduced the initial concentration required for significant adsorption $[pep]_{min}$ compared to pep1 (Figure S9a). Substitution of His-11 near the C-terminal for Ala (pep1_11) decreased adsorption to silica and increased the threshold concentration for adsorption $[pep]_{min}$ compared to pep 1. A reduction in ζ potential of the silica particles occurred upon addition of all three peptides which was somewhat smaller for pep1_11 compared to pep1_6 and pep1 (Figure S9b). Molecular dynamics simulation indicated that removal of His-6 from the middle of the peptide increased conformational flexibility among neighboring groups. As a result of the diminished backbone stiffness, pep1_6 is able to better interact with the surface from both ends, including N-terminal Lys and three His residues at the C-terminus (Figure 10b,c). The average number of hydrogen bonds to the surface through participation of several residues (Ser, Arg, Asp, His) along the backbone was also found to increase in pep1_6. In contrast, substitution of His-11 for Ala near the C-terminal end preserved backbone rigidity and reduced the number of hydrogen bonds with the surface (Figure 10b,d). The three C-terminal His residues also share the positive charge of pep1 which is less feasible in pep1_11. As a consequence, pep1_11 shows reduced ion pairing, less compensation in zeta potential, an increase in computed adsorption energy (further above zero), and an increase in initial

dx.doi.org/10.1021/ja211307u | J. Am. Chem. Soc. 2012, 134, 6244−6256

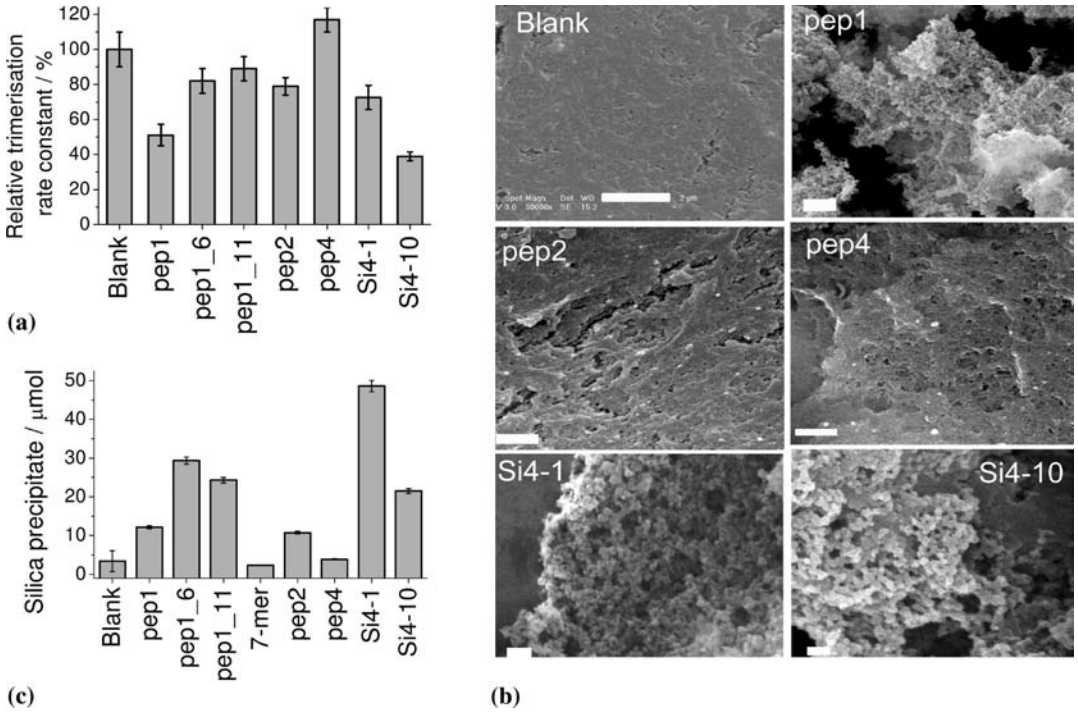

Figure 12. (a) Rate constants for trimer formation relative to the *blank* sample for selected peptides when SiCat was used as silica precursor. (b) Representative SEM images of the morphology of silica produced from SiCat in the absence (Blank) and in the presence of various peptides. Scale bars = 1 μm. (c) Amount of silica precipitated in the presence of peptides when TMOS was used as the silica precursor.

Table 4. A List of Residues Found To Be Important in Binding onto Silica Surfaces for Selected Peptides

Interactions	Pep1	Pep1_6	Pep1_11	Pep4
Strong	N-terminus, Lys_1	N-terminus, Lys_1	N-terminus, Lys_1	
Weak or Intermittent	Ser_4, Arg_5, His_6, His_{10-12}	Arg_5 Ser_2, Ser_4, Asp_7, His_8, His_{10}, His_{12}	Ser_4, $His_{10,12}$	C-terminus, Arg_{12} Arg_3

concentration for significant adsorption $[pep]_{min}$ relative to pep1. These results suggest that H-11 is a key residue while H-6 is perhaps dispensable, contrary to the notion that H-6 is important for silica binding.[17]

The proposed binding mechanism is further supported by agreement of the relative binding strength of the peptide mutants pep1, pep1_6, and pep1_11 in simulation (Table 3) and experiment (Figure 10a); computed interaction energies of individual amino acids with the surface excluding contributions by water (Figure 11a); Ramachandran plots (Figure 11b, Figure S10); and changes in computed ^1H, ^{13}C, and ^{15}N NMR spectral shifts (Figure S11).[61] Adsorption slightly increases the fraction of β strand conformations versus α helical conformations (see section S3 of the Supporting Information for further details).

The trends in adsorption of mutant peptides show that (i) binding peptide sequences for silica nanoparticles of known composition and surface acidity can be designed within a certain confidence level, (ii) the adsorption mechanism is tunable, and (iii) simulation can provide significant guidance.

In comparison to noble metal surfaces,[13−15,72] the impact of amino acid sequence on binding energies as well as conformation changes of peptides upon binding appear weaker. Previously, large differences in binding affinities upon constraining conformations of Au binding peptides[13] as well as significant changes in the secondary structure of Pd binding peptides were reported.[14,15] Weaker adhesion of peptides to silica is related to a much lower surface energy of ~200 mJ/m^2 of silica[34] in comparison to >1000 mJ/m^2 for noble metals.[76]

3.6. Silica Condensation and Precipitation. To assess possible relations between the binding strength of the identified peptides to silica nanoparticles and their activity in silica mineralization, we carried out silica precipitation experiments using SiCat and TMOS as molecular precursors. SiCat was used to monitor possible catalytic and inhibitory effects[72] of the peptides in the early stages of silicic acid condensation and to analyze the final silica precipitates. Experiments with TMOS served a rapid assessment of the amount of silica precipitated in 15 min.

In the early stages of silica mineralization, silicic acid trimers can form by reaction between a monomer and a dimer, or by reaction between three monomers. Using SiCat as a precursor, we measured the rate of disappearance of the silicic acid monomer and of the dimer in the presence of the peptides, and for a blank sample without peptide (see section S1.4 in the Supporting Information).[67,77] The decrease in silicic acid concentration over time was converted into rate constants for the formation of trimers (k_3) (Figure 12a). A significant reduction in the rate constant k_3 of 40−45% relative to the blank sample was found in the presence of pep1 and Si4-10, and no significant effects for the other peptides. The same two peptides pep1 and Si4-10 also showed the lowest $[pep]_{min}$, the strongest electrostatic interaction with the surface and largest reduction in ζ-potential upon adsorption (Figure 4), and they

dx.doi.org/10.1021/ja211307u | J. Am. Chem. Soc. 2012, 134, 6244−6256

can be considered the two strongest silica binders in this series (Figure 3a,b). The predominantly inhibitive effect of these peptides on the silicic acid condensation rate is in contrast to catalytic effects of other charged molecules (polylysine, small amines) containing multiple ammonium groups.[9,78,79]

Upon completion of the kinetic measurements with SiCat precursor, the reaction solutions were equilibrated for 7 days, followed by collection of the precipitates by centrifugation, washing, and lyophilization. Analysis of the precipitate morphologies by SEM showed materials with particulate features and particle sizes ~35, ~150, and ~230 nm in the presence of pep1, Si4-1, and Si4-10 in the condensing solutions (Figure 12b). The particles were silica−peptide hybrids as confirmed by thermal analysis (TGA) and contained over 20 wt % of occluded peptide (Figure S12). FTIR spectroscopy performed on the precipitates confirmed the presence of peptides by amide peaks in the region of 1600−1700 cm^{-1} and silica by strong peaks near 1000 cm^{-1} (Figure S13). Samples collected in the absence of added peptide (*blank*) showed continuous gels lacking particulate features and the effect of pep2 and pep4 on sample morphology was negligible, similar to the blank sample.

The precipitation of silica from TMOS was used to quantify the influence of the peptides on coagulation in shorter time. Out of the wild-type peptides identified by phage display, only Si4-1 and Si4-10 precipitated significant amounts of silica of 48 and 21 μmol, respectively (Figure 12c). Pep1 and pep2 show a low precipitation activity of 10−12 μmol, and the 7mer and pep4 show negligible activity for silica precipitation (Figure 12c). Interestingly, the mutants pep1_6 and pep1_11 precipitated more than twice the amount of silica (~25−30 μmol) compared to the wild-type pep1 (12 μmol), in the range of the activity of Si4-1 and Si4-10.

In summary, silica precipitation is affected by various kinetic factors and involves interactions between peptides and oligomeric silicate species (<1 nm), markedly different from those on extended surfaces. The choice of precursor plays a role and detailed future investigations of the condensation mechanism will be necessary to derive a correlation between peptide structure, p*I*, rate constants, and precipitation activity. Although the peptides used possessed a p*I* >8, only some were able to produce particles while the others hardly had an effect on the product morphology. A limited correlation between the binding strength and precipitation activity, however, is supported by the measurements.

4. CONCLUSIONS

We have demonstrated the importance of silica surface structure on specific binding of peptides, and identified the adsorption mechanism as a dual action of ion pairing and hydrogen bonds between peptides and the surface, complemented by ion−dipole, dipole−dipole, and van-der-Waals interactions. The degree of ionization of the silica surface is critical for selective adsorption. The area density of sodium siloxide groups increased on larger silica nanoparticles derived from modified Stöber synthesis, and intermediate cation density (~1 SiO^- Na^+ group/nm^2) maximizes the amount of dissociated sodium ions in the aqueous interfacial region on the nanoparticle surface.

The best-binding peptides in a combinatorial phage library were found to be customized for each nanoparticle type used and exhibit low sequence similarity, a notion strongly supported by the inverse correlation between pzc and peptide p*I*. The binding data for strongly cationic peptides showed strong adsorption at low initial concentration due to ion pairing, combined with a reduction in zeta potential and surface charge neutralization. Peptides without cationic groups required a higher initial threshold concentration for adsorption and showed no sign of surface saturation owing to the formation of hydrogen bonds and other nonioinc interactions. All-atomic molecular dynamics simulation with realistic surface composition ($SiOH/SiO^-Na^+$), peptide concentrations in explicit water, pH, and temperature support experimental observations and allow sensitive predictions such as the influence of point mutations upon adsorption strength.

On a molecular level, adsorption is driven by ammonium groups in N-terminal and Lys residues and further modulated by Arg residues through formation of ion pairs with siloxide groups on the silica nanoparticle surface, as well as by Ser, His, and Asp residues through hydrogen bonds and polar interactions (Table 4). Point substitutions of the silica-binding peptide KSLSRHDHIHHH in the 6th and 11th position for A were used to tune the strength of peptide binding. In particular, for pep1_6, we have shown an increase in conformational flexibility leading to stronger binding of many residues by ion pairing and hydrogen bonds, and for pep1_11, a decrease in proton distribution and number of hydrogen bonds near the C-terminal end which reduced the binding strength.

The proposed surface structure and binding mechanism can serve as a guide for the interaction of peptides, organic molecules, and polymers with silica surfaces in many fields of bioscience, engineering applications and chemistry, and enables simulation as a computational tool for the analysis of such interfacial processes. We have also found that strongly adsorbing peptides decrease the mineralization rate of silica precursors with a better chance of defined particle morphology. Awareness of the suggested molecular mechanisms offers the potential for better control over adsorption and the self-assembly of materials into hierarchical larger scale structures. The examination of self-assembly beyond the single-oligomer single-surface scale still requires substantial future work.

■ ASSOCIATED CONTENT

Supporting Information

Details of experimental and computational methods, as well as further results of measurements and simulations (3 tables and 13 figures). This material is available free of charge via the Internet at http://pubs.acs.org.

■ AUTHOR INFORMATION

Corresponding Author

carole.perry@ntu.ac.uk; hendrik.heinz@uakron.edu

Notes

The authors declare no competing financial interest.

■ ACKNOWLEDGMENTS

We acknowledge support from the US-AFOSR (FA 9550-06-1-0154 and FA 9550-10-1-0024), the Royal Society (CG072089), the Air Force Research Laboratory, Wright-Patterson AFB (WPAFB), the National Science Foundation (DMR-0955071), the University of Akron, the Ohio Department of Development, as well as the allocation of computer resources at the Ohio Supercomputing Center and at WPAFB. We thank Dr. Paul Roach for kindly providing silica samples, Ms. Yulia Nigmatulina for help in developing peptide quantification assays, Dr. Joe Slocik, AFRL for XPS analysis and Dr. Valeria Puddu and Dr. David J. Belton for numerous helpful discussions.

REFERENCES

(1) (a) Hench, L. L. *J. Am. Ceram. Soc.* **1991**, *74*, 1487−1510. (b) Kresge, C. T.; Leonowicz, M. E.; Roth, W. J.; Vartuli, J. C.; Beck, J. S. *Nature* **1992**, *359*, 710−712. (c) Kendall, T. *Industrial Minerals* **2000**, March, 49−59.

(2) (a) Simkiss, K.; Wilbur, K. M. *Biomineralization*; Academic Press: San Diego, CA, 1989. (b) *Biomineralization: From Biology to Biotechnology and Medical Application*; Baeuerlein, E., Ed.; Wiley-VCH: Chichester, 2000. (c) Hildebrand, M. *Prog. Org. Coat.* **2003**, *47*, 256−266. (d) Hildebrand, M. *Chem. Rev.* **2008**, *108*, 4855−4874.

(3) Mann, S., *Biomineralization: Principles and Concepts in Bioinorganic Materials Chemistry*; Oxford University Press: New York, 2001.

(4) Yin, Y.; Alivisatos, A. P. *Nature* **2005**, *437*, 664−670.

(5) Patwardhan, S. V.; Mukherjee, N.; Steinitz-Kannan, M.; Clarson, S. J. *Chem. Commun.* **2003**, *10*, 1122−1123.

(6) Belton, D.; Paine, G.; Patwardhan, S. V.; Perry, C. C. *J. Mater. Chem.* **2004**, *14*, 2231−2241.

(7) Patwardhan, S. V.; Clarson, S. J.; Perry, C. C. *Chem. Commun.* **2005**, 1113−1121.

(8) Brott, L. L.; Pikas, D. J.; Naik, R. R.; Kirkpatrick, S. M.; Tomlin, D. W.; Whitlock, P. W.; Clarson, S. J.; Stone, M. O. *Nature* **2001**, *413*, 291−293.

(9) (a) Patwardhan, S. V.; Shiba, K.; Raab, C.; Husing, N.; Clarson, S. J. In *Polymer Biocatalysis and Biomaterials*; Cheng, H. N., Gross, R. A., Eds.; Oxford University Press: Washington, DC, 2005. (b) Patwardhan, S. V.; Shiba, K.; Schroder, H. C.; Muller, W. E. G.; Clarson, S. J.; Perry, C. C. In *The Science and Technology of Silicones and Silicone-Modified Materials*; Clarson, S. J., Fitzgerald, J. J., Owen, M. J., Smith, S. D., Van Dyke, M. E., Eds.; American Chemical Society: Washington, DC, 2007; Vol. *964*. (c) Weidner, T.; Breen, N. F.; Drobny, G. P.; Castner, D. G. *J. Phys. Chem. B* **2009**, *113*, 15423−15426.

(10) Dickerson, M. B.; Sandhage, K. H.; Naik, R. R. *Chem. Rev.* **2008**, *108*, 4935−4978.

(11) Patwardhan, S. V.; Patwardhan, G.; Perry, C. C. *J. Mater. Chem.* **2007**, *17*, 2875−2884.

(12) (a) Sano, K. I.; Shiba, K. *J. Am. Chem. Soc.* **2003**, *125*, 14234−14235. (b) Chen, H. B.; Su, X. D.; Neoh, K. G.; Choe, W. S. *Langmuir* **2008**, *24*, 6852−6857. (c) Skelton, A. A.; Liang, T. N.; Walsh, T. R. *ACS Appl. Mater. Interfaces* **2009**, *1*, 1482−1491.

(13) Hnilova, M.; Oren, E. E.; Seker, U. O. S.; Wilson, B. R.; Collino, S.; Evans, J. S.; Tamerler, C.; Sarikaya, M. *Langmuir* **2008**, *24*, 12440−12445.

(14) Heinz, H.; Farmer, B. L.; Pandey, R. B.; Slocik, J.; Patnaik, S. S.; Pachter, R.; Naik, R. R. *J. Am. Chem. Soc.* **2009**, *131*, 9704−9714.

(15) Coppage, R.; Slocik, J. M.; Sethi, M.; Pacardo, D. B.; Naik, R. R.; Knecht, M. R. *Angew. Chem., Int. Ed.* **2010**, *49*, 3767−3770.

(16) Naik, R. R.; Brott, L. L.; Clarson, S. J.; Stone, M. O. *J. Nanosci. Nanotechnol.* **2002**, *2*, 95−100.

(17) Eteshola, E.; Brillson, L. J.; Lee, S. C. *Biomol. Eng.* **2005**, *22*, 201−204.

(18) Oren, E. E.; Notman, R.; Kim, I. W.; Evans, J. S.; Walsh, T. R.; Samudrala, R.; Tamerler, C.; Sarikaya, M. *Langmuir* **2010**, *26*, 11003−11009.

(19) Naik, R. R.; Jones, S. E.; Murray, C. J.; McAuliffe, J. C.; Vaia, R. A.; Stone, M. O. *Adv. Funct. Mater.* **2004**, *14*, 25−30.

(20) Willett, R. L.; Baldwin, K. W.; West, K. W.; Pfeiffer, L. N. *Proc. Natl. Acad. Sci. U.S.A.* **2005**, *102*, 7817−7822.

(21) Liang, M. K.; Deschaume, O.; Patwardhan, S. V.; Perry, C. C. *J. Mater. Chem.* **2011**, *21*, 80−89.

(22) (a) Erdem, B.; Hunsicker, R. A.; Simmons, G. W.; Sudol, E. D.; Dimonie, V. L.; El-Aasser, M. S. *Langmuir* **2001**, *17*, 2664−2669. (b) Brown, M. A.; Huthwelker, T.; Redondo, A. B.; Janousch, M.; Faubel, M.; Arrell, C. A.; Scarongella, M.; Chergui, M.; van Bokhoven, J. A. *J. Phys. Chem. Lett.* **2012**, *3*, 231−235.

(23) Dettin, M.; Bagno, A.; Gambaretto, R.; Iucci, G.; Conconi, M. T.; Tuccitto, N.; Menti, A. M.; Grandi, C.; Di Bello, C.; Licciardello, A.; Polzonetti, G. *J. Biomed. Mater. Res., Part B* **2009**, *90A*, 35−45.

(24) (a) Weidner, T.; Breen, N. F.; Li, K.; Drobny, G. P.; Castner, D. G. *Proc. Natl. Acad. Sci. U.S.A.* **2010**, *107*, 13288−13293. (b) Nguyen, K. T.; Soong, R.; Im, S.-C.; Waskell, L.; Ramamoorthy, A.; Chen, Z. *J. Am. Chem. Soc.* **2010**, *132*, 15112−15115.

(25) Bolt, G. H. *J. Phys. Chem.* **1957**, *61*, 1166−1169.

(26) Abendroth, R. P. *J. Colloid Interface Sci.* **1970**, *34*, 591−596.

(27) Yates, D. E.; Healy, T. W. *J. Colloid Interface Sci.* **1976**, *55*, 9−19.

(28) Milonjic, S. K. *Colloids Surf.* **1987**, *23*, 301−312.

(29) Zerrouk, R.; Foissy, A.; Mercier, R.; Chevallier, Y.; Morawski, J. C. *J. Colloid Interface Sci.* **1990**, *139*, 20−29.

(30) House, W. A.; Orr, D. R. *J. Chem. Soc., Faraday Trans.* **1992**, *88*, 233−241.

(31) Sonnefeld, J. *J. Colloid Interface Sci.* **1996**, *183*, 597−599.

(32) Mendez, A.; Bosch, E.; Roses, M.; Neue, U. D. *J. Chromatogr., A* **2003**, *986*, 33−44.

(33) Zhuravlev, L. T. *Colloids Surf., A* **2000**, *173*, 1−38.

(34) Helmy, A. K.; de Bussetti, S. G.; Ferreiro, E. A. *Appl. Surf. Sci.* **2007**, *253*, 6878−6882.

(35) Sanders, M. J.; Leslie, M.; Catlow, C. R. A. *J. Chem. Soc., Chem. Commun* **1984**, 1271−1273.

(36) Feuston, B. P.; Garofalini, S. H. *J. Chem. Phys.* **1988**, *89*, 5818−5824.

(37) van Beest, B. W. H.; Kramer, G. J.; van Santen, R. A. *Phys. Rev. Lett.* **1990**, *64*, 1955−1958.

(38) Heinz, H.; Castelijns, H. J.; Suter, U. W. *J. Am. Chem. Soc.* **2003**, *125*, 9500−9510.

(39) Heinz, H.; Suter, U. W. *J. Phys. Chem. B* **2004**, *108*, 18341−18352.

(40) (a) Gambino, G. L.; Lombardo, G. M.; Grassi, A.; Marletta, G. *J. Phys. Chem. B* **2004**, *108*, 2600−2607. (b) Raut, V. P.; Agashe, M. A.; Stuart, S. J.; Latour, R. A. *Langmuir* **2005**, *21*, 1629−1639.

(41) Heinz, H.; Koerner, H.; Anderson, K. L.; Vaia, R. A.; Farmer, B. L. *Chem. Mater.* **2005**, *17*, 5658−5669.

(42) Lopes, P. E. M.; Murashov, V.; Tazi, M.; Demchuk, E.; MacKerell, A. D. *J. Phys. Chem. B* **2006**, *110*, 2782−2792.

(43) He, Y.; Cao, C.; Wan, Y. X.; Cheng, H. P. *J. Chem. Phys.* **2006**, *124*, 024722.

(44) Heinz, H.; Vaia, R. A.; Farmer, B. L. *J. Chem. Phys.* **2006**, *124*, 224713.

(45) Cruz-Chu, E. R.; Aksimentiev, A.; Schulten, K. *J. Phys. Chem. B* **2006**, *110*, 21497−21508.

(46) Rimola, A.; Civalleri, B.; Ugliengo, P. *Langmuir* **2008**, *24*, 14027−14034.

(47) Argyris, D.; Cole, D. R.; Striolo, A. *J. Phys. Chem. C* **2009**, *113*, 19591−19600.

(48) Heinz, H. *J. Comput. Chem.* **2010**, *31*, 1564−1568.

(49) Vellore, N. A.; Yancey, J. A.; Collier, G.; Latour, R. A.; Stuart, S. J. *Langmuir* **2010**, *26*, 7396−7404.

(50) Feng, J.; Pandey, R. B.; Berry, R. J.; Farmer, B. L.; Naik, R. R.; Heinz, H. *Soft Matter* **2011**, *7*, 2113−2120.

(51) Li, X. F.; Latour, R. A. *J. Comput. Chem.* **2011**, *32*, 1096−1100.

(52) Feng, J.; Slocik, J. M.; Sarikaya, M.; Naik, R. R.; Farmer, B. L.; Heinz, H. *Small* **2012**, *8*, DOI: 10.1002/smll.201102066.

(53) (a) Heinz, H.; Vaia, R. A.; Krishnamoorti, R.; Farmer, B. L. *Chem. Mater.* **2007**, *19*, 59−68. (b) Heinz, H.; Vaia, R. A.; Koerner, H.; Farmer, B. L. *Chem. Matter.* **2008**, *20*, 6444−6456. (c) Fu, Y. T.; Heinz, H. *Chem. Mater.* **2010**, *22*, 1595−1605.

(54) Heinz, H.; Vaia, R. A.; Farmer, B. L.; Naik, R. R. *J. Phys. Chem. C* **2008**, *112*, 17281−17290.

(55) Stöber, W.; Fink, A.; Bohn, E. *J. Colloid Interface Sci.* **1968**, *26*, 62.

(56) Roach, P.; Farrar, D.; Perry, C. C. *J. Am. Chem. Soc.* **2006**, *128*, 3939−3945.

(57) *Fmoc Solid Phase Peptide Synthesis: A Practical Approach*; Chan, W. C.; White, P. D., Eds.; Oxford University Press: Oxford, 2000.

(58) Noble, J. E.; Knight, A. E.; Reason, A. J.; Di Matola, A.; Bailey, M. J. A. *Mol. Biotechnol.* **2007**, *37*, 99−111.

(59) Plimpton, S. *J. Comput. Phys.* **1995**, *117*, 1−19.

(60) *Materials Studio 4.1 and Discover program*; Acelrys, Inc.: San Diego, CA, 2006.
(61) Neal, S.; Nip, A. M.; Zhang, H. Y.; Wishart, D. S. *J. Biomol. NMR* **2003**, *26*, 215−240.
(62) ClustalW2, European Bioinformatics Institute Home Page. www.ebi.ac.uk/clustalw, 2008.
(63) Perry, C. C.; Patwardhan, S. V.; Deschaume, O. *Biochem. Soc. Trans.* **2009**, *37*, 687−691.
(64) (a) Naik, R. R.; Stringer, S. J.; Agarwal, G.; Jones, S. E.; Stone, M. O. *Nat. Mater.* **2002**, *1*, 169−172. (b) Whaley, S. R.; English, D. S.; Hu, E. L.; Barbara, P. F.; Belcher, A. M. *Nature* **2000**, *405*, 665−668. (c) Braun, R.; Sarikaya, M.; Schulten, K. *J. Biomater. Sci., Polym. Ed.* **2002**, *13*, 747−757.
(65) Chiu, C. Y.; Li, Y. J.; Ruan, L. Y.; Ye, X. C.; Murray, C. B.; Huang, Y. *Nat. Chem.* **2011**, *3*, 393−399.
(66) ExPasy Home Page. www.expasy.org.
(67) Iler, R. K. *The Chemistry of Silica: Solubility, Polymerization, Colloid and Surface Properties, And Biochemistry*; Wiley: New York, 1979.
(68) Rosen, M. J. *J. Am. Oil Chem. Soc.* **1975**, *52*, 431−435.
(69) (a) Liu, Y.; Xu, H.; Tay, J. H. *J. Environ. Eng.* **2005**, *131*, 1466−1468. (b) Skopp, J. *J. Chem. Educ.* **2009**, *86*, 1341−1343. (c) Wang, J.; Zheng, S.; Liu, J.; Xu, Z. *Chem. Eng. J* **2010**, *165*, 10−16.
(70) The surface coverage with peptide can be estimated from the number of adsorbed peptides per nm^2 particle surface area (see Figure 3a,b) times the approximate van-der-Waals area of an extended peptide, which equals 2−3 nm^2 according to the atomistic models.
(71) (a) Eby, D. M.; Johnson, G. R.; Farmer, B. L.; Pandey, R. B. *Phys. Chem. Chem. Phys.* **2010**, *13*, 1123−1130. (b) Kröger, N.; Lorenz, S.; Brunner, E.; Sumper, M. *Science* **2002**, *298*, 584−586.
(72) Mijajlovic, M.; Biggs, M. J. *J. Phys. Chem. C* **2007**, *111*, 15839−15847.
(73) Mermut, O.; Phillips, D. C.; York, R. L.; McCrea, K. R.; Ward, R. S.; Somorjai, G. A. *J. Am. Chem. Soc.* **2006**, *128*, 3598−3607.
(74) Bailey, S. W. Hydrous Phyllosilicates. In *Reviews in Mineralogy*; Mineralogical Society of America: Chelsea, MI, 1988; Vol. *19*.
(75) Zhou, Y.; Shimizu, K.; Cha, J. N.; Stucky, G. D.; Morse, D. E. *Angew. Chem., Int. Ed.* **1999**, *38*, 779−782.
(76) Tyson, W. R.; Miller, W. A. *Surf. Sci.* **1977**, *62*, 267−276.
(77) Belton, D. J.; Deschaume, O.; Patwardhan, S. V.; Perry, C. C. *J. Phys. Chem. B* **2010**, *114*, 9947−9955.
(78) Coradin, T.; Livage, J. *Colloids Surf., B* **2001**, *21*, 329−336.
(79) Belton, D. J.; Patwardhan, S. V.; Annenkov, V. V.; Danilovtseva, E. N.; Perry, C. C. *Proc. Natl. Acad. Sci. U.S.A.* **2008**, *105*, 5963−5968.